Sensors and Materials, Vol. 34, No. 11 (2022) 4001–4016
MYU Tokyo

S & M 3092

Cyclically Shifted Extreme-point Symmetric Mode Decomposition (CS-ESMD)-based Progressive Denoising Approach for Ground-based Synthetic Aperture Radar Bridge Health Monitoring Signals

Runjie Wang,[1] Yimeng Huang,[1] Xianglei Liu,[1*] Hui Wang,[2] and Mengzhuo Jiang[3]

[1]Key Laboratory for Urban Geomatics of National Administration of Surveying, Mapping and Geoinformation, Beijing University of Civil Engineering and Architecture, 1 Zhanlanguan Road, Beijing 100048, China
[2]Beijing Urban Construction Exploration & Surveying Design Research Institute Co., Ltd., 6 Anhuili Fifth District, Beijing 100101, China
[3]Leica Geosystems Trade (Beijing) Co., Ltd., No. 16 Chao Yang Men Wai Street, Chaoyang District, Beijing 100020, China

(Received July 3, 2022; accepted September 13, 2022)

Keywords: ground-based synthetic aperture radar, progressive denoising, extreme-point symmetric mode decomposition, cyclically shifted, bridge dynamic deflection

Ground-based synthetic aperture radar (GB-SAR) has a wide range of applications in bridge health detection by monitoring dynamic deflection data. However, the collected dynamic deflection signals are easily subjected to interference by noises during GB-SAR monitoring due to ground motion and complex traffic factors. It is also difficult to accurately eliminate the influence of noises by using the traditional modal decomposition method. Therefore, we propose a cyclically shifted extreme-point symmetric mode decomposition (CS-ESMD)-based progressive denoising approach, which can accurately identify high/low-frequency noise information from dynamic deflection signals through a progressive process. First, CS-ESMD is used to construct virtual multi-channel signals for the following progressive denoising process. Second, ESMD is performed on multi-channel dynamic deflection data to separate useful and high-frequency noise information. Finally, the low-frequency noises and the residual high-frequency noises are further identified and removed by second-order blind identification (SOBI) and the fast Fourier transform (FFT) method. Through simulation and practical experiments, we show that the accuracy of the progressive denoising method can be increased by 37.2% compared with traditional methods, which shows its effectiveness in improving the precision of GB-SAR dynamic deflection signals.

1. Introduction

Dynamic deflection is one of the important indexes for bridge health monitoring. It has become a research hotspot for obtaining the dynamic deflection of bridges quickly and accurately.(1) Ground-based synthetic aperture radar (GB-SAR) is a novel form of ground

*Corresponding author: e-mail: liuxianglei@bucea.edu.cn
https://doi.org/10.18494/SAM4008

ISSN 0914-4935

microwave interference technology with the advantages of high precision (0.01 mm), high sampling frequency (1000 Hz), and overall monitoring.[2,3] It can achieve sub-millimeter-level micro-deformation monitoring without contact with the observational target. It can also solve many problems of traditional bridge monitoring technology, such as a small measuring range, short measuring distance, low accuracy, and environmental impact. Thus, GB-SAR has been widely used in bridge dynamic deflection monitoring.[4–6] However, bridge dynamic deflection monitoring with GB-SAR is inevitably affected by noise factors such as ground motion and complex traffic (such as from the subway, vehicles, and pedestrians passing through the radar beam), which reduce the measurement accuracy of bridge dynamic deflection. It is critical to investigate a denoising approach that can acquire high-precision dynamic deflection signals using GB-SAR.

Only one GB-SAR device is commonly used to monitor the dynamic deflection of a bridge due to its cost and the on-site monitoring environment. Thus, only single-channel monitoring data is acquired. In this study, we conduct research based on single-channel monitoring signals. The widely used denoising approaches mainly include the wavelet transform (WT),[7,8] singular value decomposition (SVD),[9] and empirical mode decomposition (EMD).[10] The WT achieves denoising by removing the wavelet coefficients of noises and reconstructing the other wavelet coefficients based on a single wavelet threshold. Wavelet threshold criteria are different for different noise frequency scales and need to be set manually. However, a single wavelet threshold criterion cannot fully consider the signal and noise distributions. That is, it is difficult to completely eliminate the noise information with different frequency scales. The above reasons reduce the adaptability of the WT method, making it unsuitable for monitoring bridge dynamic deflection signals monitored by GB-SAR.[11] The SVD method converts nonstationary or nonlinear signals into matrices and performs SVD on them. Since the singular values corresponding to signals and noises are different, the selection of appropriate singular values can effectively separate noise information from signals containing noises.[1] However, the denoising accuracy depends on how the effective rank order is selected and how the structure of the reconstruction matrix is determined. Moreover, the signal denoised by SVD has a small phase shift, which limits the applicability of the method.[12,13]

EMD can adaptively decompose the original signal into a series of intrinsic mode function (IMF) components, making it suitable for nonstationary and nonlinear signals. It is widely used in the field of signal denoising.[14] However, modal aliasing and the endpoint effect exist in this method. Ensemble empirical mode decomposition (EEMD) is an improved method for solving the modal aliasing problems in EMD.[15] It takes the EMD algorithm as the core and repeatedly adds a white noise of finite amplitude to the original signal for multiple decomposition. Then it takes the average value obtained through multiple decomposition to reduce the problem of modal aliasing. However, it is difficult to reduce the influence of instantaneous noises in EEMD.[16,17] Extreme-point symmetric mode decomposition (ESMD) inherits the adaptability of EMD and is suitable for nonstationary and nonlinear signal processing.[18,19] Compared with EMD, its internal mean square has a smaller amplitude, which can effectively reduce the uncertainty caused by interpolation. In addition, the problems of modal aliasing and the endpoint effect can be effectively solved. However, the principle of signal denoising using modal decomposition

methods such as EMD, EEMD, and ESMD is to reduce the impact of noise by eliminating a certain number of low-order IMF components with relatively high frequency features.[10] The remaining IMF components will inevitably have low-frequency noises and some high-frequency residual noises. Therefore, it is difficult to accurately eliminate the influence of noises by using traditional modal decomposition methods.

In view of the above problems, in some studies, the traditional modal decomposition method has been combined with second-order blind identification (SOBI) to denoise the monitoring signal and achieve better denoising effects. For example, Liu *et al.* proposed a denoising approach based on a combination of EEMD, ESMD, and SOBI for GB-SAR bridge dynamic deflection signals.[20] They experimentally showed that their method had a better denoising effect than traditional modal decomposition methods alone. However, to solve the underdetermination problem existing in the SOBI denoising process when using single-channel GB-SAR dynamic deflection data, virtual multi-channel monitoring signals are first constructed. Liu *et al.* adopted EEMD and ESMD to decompose the original signals. Then the original signals were combined with decomposed parts to construct virtual multi-channel data. Nevertheless, the multi-channel extended data had been subjected to EEMD and ESMD as well as high-frequency noise removal, which may cause the loss of useful data. Therefore, to solve the above problems, cyclically shifted ESMD (CS-ESMD) is proposed in this study as a method for virtual multi-channel data construction. Then a progressive denoising model based on SOBI and the fast Fourier transform (FFT) is built. Four critical items are investigated as follows: (i) CS-ESMD is proposed as a method to construct virtual multi-channel dynamic deflection signals. First, a series of IMF components is generated by ESMD. Then the IMF_1 component is cyclically shifted to obtain multiple groups of different noise components. The noise components obtained by cyclic shifting and other IMF components are superimposed to obtain new virtual multi-channel observation signals. (ii) Several groups of new multi-channel observation signals are decomposed by ESMD to distinguish the high- and low-frequency IMF components based on Spearman's Rho. Then the high-frequency IMF components are removed to achieve preliminary GB-SAR signal denoising. (iii) The low-frequency noises and the residual high-frequency noise components are further identified and removed by combining SOBI and the FFT. (iv) A simulation experiment and practical experiment are conducted to verify the validity of the proposed method. The remainder of the paper is organized as follows. In Sect. 2, the proposed CS-ESMD approach is introduced in detail. In Sect. 3, the simulation experiment and practical experiment are described. Section 4 presents the conclusions.

2. Methodology

Figure 1 shows the overall flow of the proposed CS-ESMD-based progressive denoising approach, which includes three key technologies: (1) CS-ESMD is performed on the original GB-SAR bridge dynamic deflection signal to obtain virtual multi-channel signals. (2) ESMD is used to decompose the multi-channel signals, and Spearman's Rho is applied to separate and remove the high-frequency noises. (3) SOBI and the FFT are then employed to eliminate low-frequency noises and residual high-frequency noises.

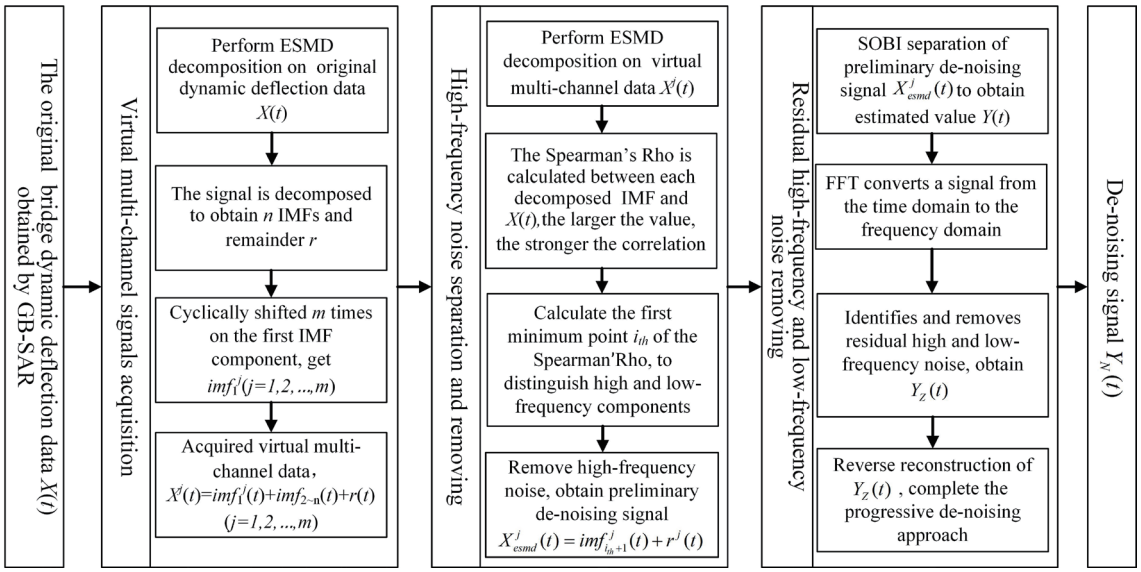

Fig. 1. Technical and analytical framework of CS-ESMD-based progressive denoising approach.

2.1 Acquisition of virtual multi-channel GB-SAR dynamic deflection signals

Owing to the cost of the instrument and the on-site monitoring environment, we use only one GB-SAR device to monitor bridge dynamic deflection. Thus, only single-channel monitoring data is acquired. CS-ESMD is proposed to extend the single-channel signal to virtual multi-channel signals. First, the original signal is decomposed by ESMD to generate a series of IMF components and remainder *r*. Then, the IMF_1 component is cyclically shifted to obtain multiple groups of different noise components. After cyclic shifting, the signal has a different shape but its power remains unchanged. By using cyclic shifting, multiple groups of IMF_1 components can be obtained. The new components are then superimposed on the remaining IMFs to obtain multi-channel signals with a constant signal-to-noise ratio (SNR). As ESMD is a commonly used and mature algorithm, it will be not repeated here. The detailed algorithm of ESMD can be found in Ref. 20. The specific process of CS-ESMD is as follows:

(1) Perform ESMD on the original signal $X(t)$ to obtain n components $imf(t)$ and remainder $r(t)$:

$$X(t)=\sum_{i=1}^{n} imf_i(t)+r(t). \tag{1}$$

(2) Perform m cyclic shifts on the first IMF component $imf_1(t)$ to obtain m groups of new components:

$$imf_1^j(t)=circulate(imf_1(t)), \qquad j=1, 2, ..., m, \tag{2}$$

where j represents the number of cycles and $imf_1^j(t)$ represents the new component generated by cycle j.
(3) Superimpose the new noise component $imf_1^j(t)$ generated by cyclic shifting on the remaining IMF components to obtain m groups of new multi-channel signals:

$$X^j(t) = imf_1^j(t) + \sum_{i=2}^{n} imf_i(t) + r(t), \qquad j = 1, 2, ..., m. \tag{3}$$

2.2 High-frequency noise separation and removal

The original signal can be decomposed into a series of IMF components from high frequency to low frequency using ESMD. The high-frequency noises are always centered on the lower-order IMF components. Therefore, the impact of high-frequency noises on GB-SAR signals can be effectively reduced by identifying and removing these IMF components. Spearman's Rho is a commonly used basis to separate high-frequency and low-frequency IMF components. It uses the ranks of two variables to analyze variable elements and to measure the closeness of the correlation between them. For each IMF component, the more noise it contains, the lower the correlation it has with the original signal. Thus, the IMF dominated by the signal has a greater correlation with the original signal. In this study, the multi-channel signals are first decomposed by ESMD to obtain IMF components. Then Spearman's Rho is used to distinguish between the IMF components dominated by noise and the IMF components dominated by the signal. The specific steps are as follows:
(1) Perform ESMD on m groups of new multi-channel data to obtain a series of IMF components:

$$X^j(t) = \sum_{i=1}^{n} imf_i^j(t) + r^j(t), \qquad j = 1, 2, ..., m, \tag{4}$$

where $imf_i^j(t)$ represents the IMF component generated by ESMD of the jth group of multi-channel data.
(2) For each group of IMFs, calculate Spearman's Rho between each IMF and the noisy signal to remove high-frequency noise information. Spearman's Rho has a range of [−1, 1], where the larger the value, the stronger the correlation with the original signal. It is calculated as follows:[21,22]

$$SP(i) = \rho(X(t), IMF_i(t)) = 1 - \frac{6\sum_{i=1}^{N}(X(t) - IMF_i(t))^2}{(N^2 - 1)N}. \tag{5}$$

In Eq. (5), $X(t)$ is the original observation signal, $IMFi(t)$ is the ith IMF component generated by ESMD of the original observation signal, and N is the signal length.

The basic principle of determining the cut-off point is to find the position where Spearman's Rho develops in the opposite direction, meaning that the correlation between the IMF and the original observation signal has changed from gradually decreasing to gradually increasing. This position is denoted as *i*th.

(3) For m groups of multi-channel data, remove the IMF components dominated by high-frequency noise:

$$X_{esmd}^{j}(t) = \sum_{i=i_{th}+1}^{n_j} imf_i^j(t) + r^j(t), \tag{6}$$

where *i*th represents the demarcation point between the high- and low-frequency components, and $X_{esmd}^{j}(t)$ represents the signal of the *j*th group after removing the high-frequency noise information.

2.3 Removal of low-frequency and residual high-frequency noises

Since there are different degrees of noise information in the IMFs generated by ESMD, the remaining IMF components will inevitably contain residual high-frequency noise and low-frequency noise information after only removing the IMF components dominated by high-frequency noise. In this study, the noise information and useful information can be regarded as different sources of information. The SOBI algorithm, as shown in Fig. 2, can use a small amount of prior information data to process the observed mixed signal by using the joint approximate diagonalization of the source signal time correlation and the covariance matrix to estimate the source signals.[23,24] It can estimate the number of source signals and separate Gaussian white noise. This algorithm does not have the problem of modal aliasing and is a robust algorithm. Therefore, in this study, the SOBI algorithm combined with the FFT is used to further process the residual high- and low-frequency noises in the signals. The specific steps are as follows:

(1) Use the SOBI algorithm to perform blind source separation (BSS) processing on the signal $X_{esmd}^{j}(t)$ from which the high-frequency noise information has already been removed. The mixing matrix A and the estimated source signal $Y(t)$ can be obtained.

(2) Use the FFT to identify the noise components in the separated source signal, which can be removed. The mixing matrix is used to inversely reconstruct the separated source signal to obtain the denoised signals.[25]

$$Y_N(t) = \boldsymbol{A} * Y_Z(t) \tag{7}$$

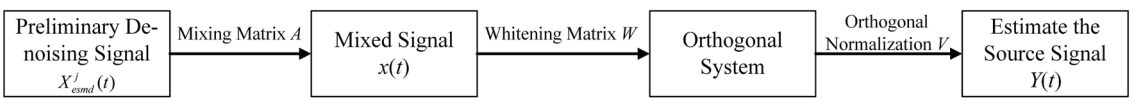

Fig. 2. Schematic diagram of SOBI.

Here, $Y_Z(t)$ represents the separated source signal with the noise components removed, A represents the estimated value of the mixing matrix, and $Y_N(t)$ is the final denoised signal.

3. Experiment and Analysis

3.1 Simulation experiment and analysis

To verify the feasibility of the denoising method proposed in this study, a simulation experiment is first conducted. The simulation signal $x(t)$ consists of the useful signal $s(t)$ and Gaussian white noise $n(t)$ [Eq. (8)]. To make it more similar to real bridge dynamic deflection data obtained by GB-SAR, $s(t)$ includes a stationary signal $s_1(t)$ and a nonstationary signal $s_2(t)$ [Eq. (9)]. The SNR of the Gaussian white noise is 20 dB. The corresponding waveforms are shown in Fig. 3.

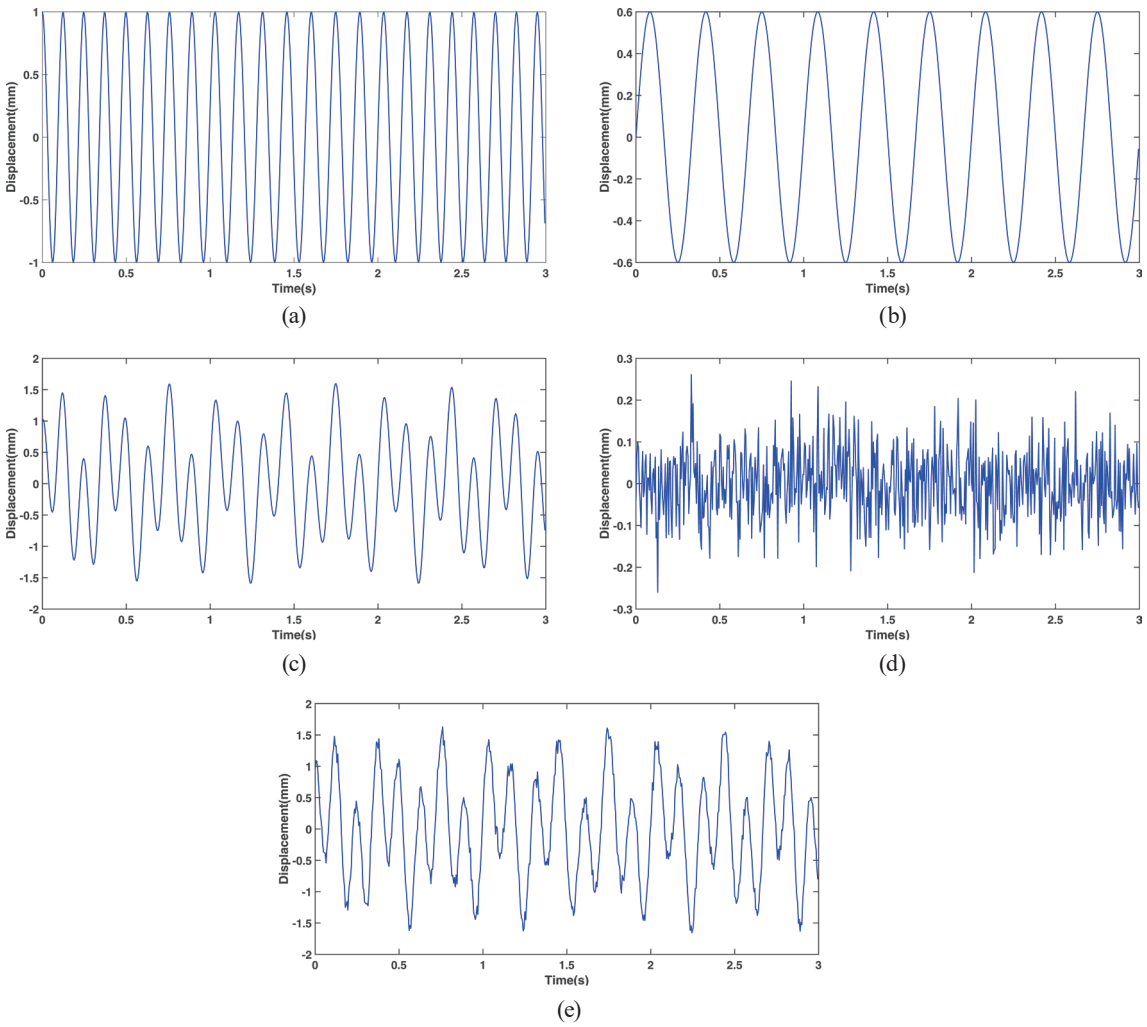

Fig. 3. (Color online) (a)–(d) Signal components $s_1(t)$, $s_2(t)$, $s(t)$, and $n(t)$, respectively. (e) Simulation signal $x(t)$.

$$x(t) = s(t) + n(t) \tag{8}$$

$$\begin{cases} s_1(t) = \cos(15\pi t + 2\sin(2t)) \\ s_2(t) = 0.6\sin(6\pi t) \\ s(t) = s_1(t) + s_2(t) \end{cases} \tag{9}$$

The data sampling frequency is 200 Hz and the number of sampling points is 1000.

As shown in Fig. 4, the ESMD method decomposed the original $x(t)$ into six IMFs and one remainder curve. The IMF_1 component was cyclically shifted to generate three sets of new noise components, as shown in Fig. 5. Figure 6 shows the three-channel signals constructed by using the three groups of new noise components generated by cyclic shifting. It can be seen from the figures that the three-channel signals had the same waveform characteristics as the original simulation signal. To further analyze the signal characteristics, these three-channel signals were

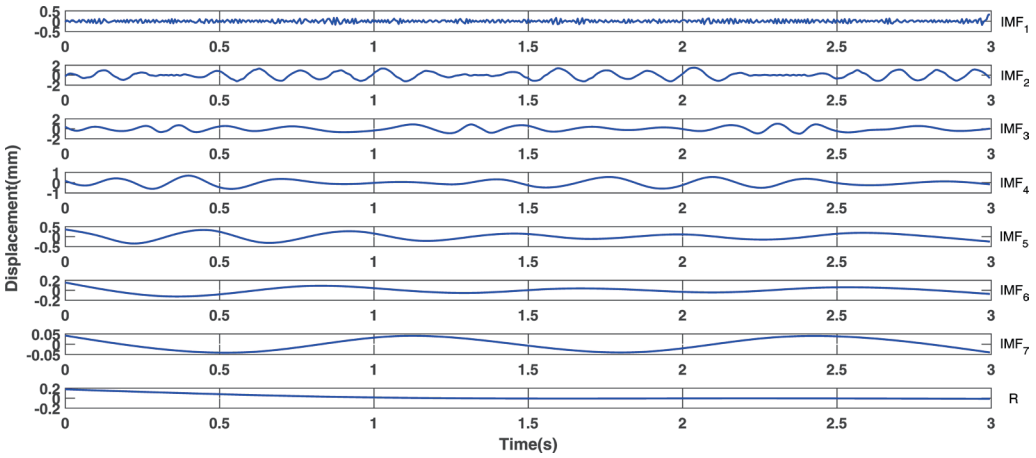

Fig. 4. (Color online) ESMD of simulated signal $x(t)$.

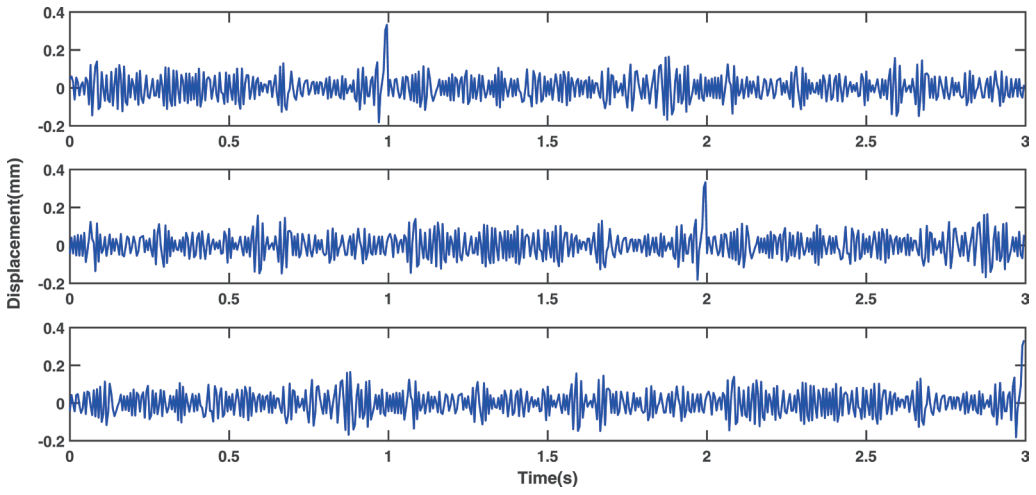

Fig. 5. (Color online) Cyclically shifted IMF1 component.

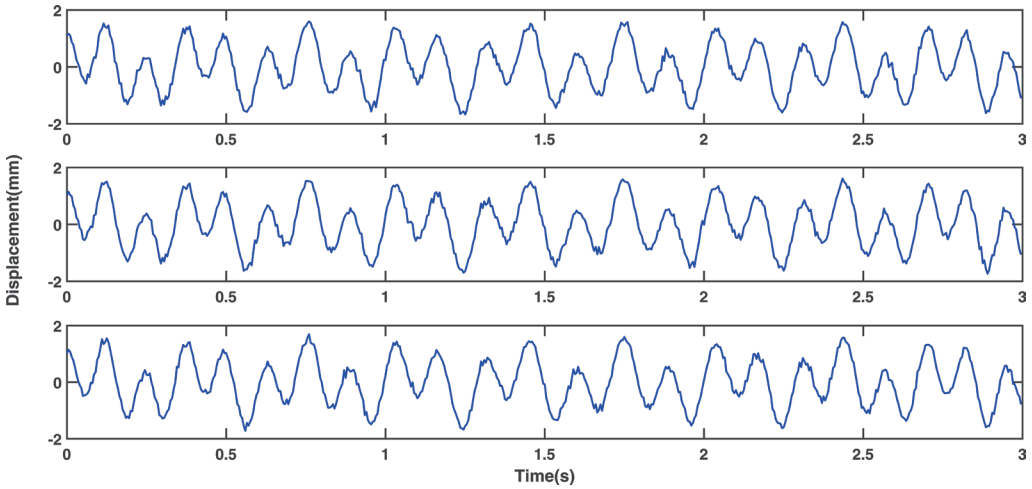

Fig. 6. (Color online) Three-channel signals.

processed by the FFT and compared with the spectrum of the original simulated signal $x(t)$. Figure 7 shows the spectrograms of the original simulation signal $x(t)$ [Fig. 7(a)] and multi-channel signals [Fig. 7(b)]. After comparison and analysis, it was found that the multi-channel signals have the same main frequencies (3 and 7.333 Hz) as the original simulation signal $x(t)$ and the spectrum characteristics are basically consistent. This further shows that three-channel signals retain all the useful information of the simulation signal $x(t)$, with only differences in the noise morphology between them.

Then, the three-channel signals generated by cyclic shifting were decomposed by ESMD. Spearman's Rho was used to distinguish high- and low-frequency components and to remove high-frequency noise components. The result is shown in Fig. 8.

The BSS method was used to remove the residual high-frequency noises, after which only low-frequency noise existed in the multi-channel signals. This method involved a combination of SOBI and the FFT. Figure 9 shows the results of denoising using the BSS method. It can be seen that separated component 1 had the same waveform change and opposite direction characteristics from the original simulation signal $x(t)$, indicating that component 1 is useful information. Separated components 2 and 3 were disordered in the time domain and may be noise components. For further verification, the FFT was performed on the separated components to obtain the spectrum, in which the time domain problem was transformed into a frequency domain problem. Figure 10 shows the frequency spectrum of the components after SOBI separation. It can be seen that separated component 1 had main frequencies of 3 and 7.333 Hz, consistent with the original simulation signal $x(t)$. Separated components 2 and 3 had no main frequency features in the frequency domain. The frequency peaks of components 2 and 3 were mainly concentrated at 0–50 Hz and 0–60 Hz, respectively, and the peaks were noisy and disordered. This revealed that separated components 2 and 3 were residual high-frequency and low-frequency noise information and separated component 1 was useful information. Then the noise information can be removed. The progressive denoising approach was used to improve the accuracy of the GB-SAR bridge dynamic deflection signal.

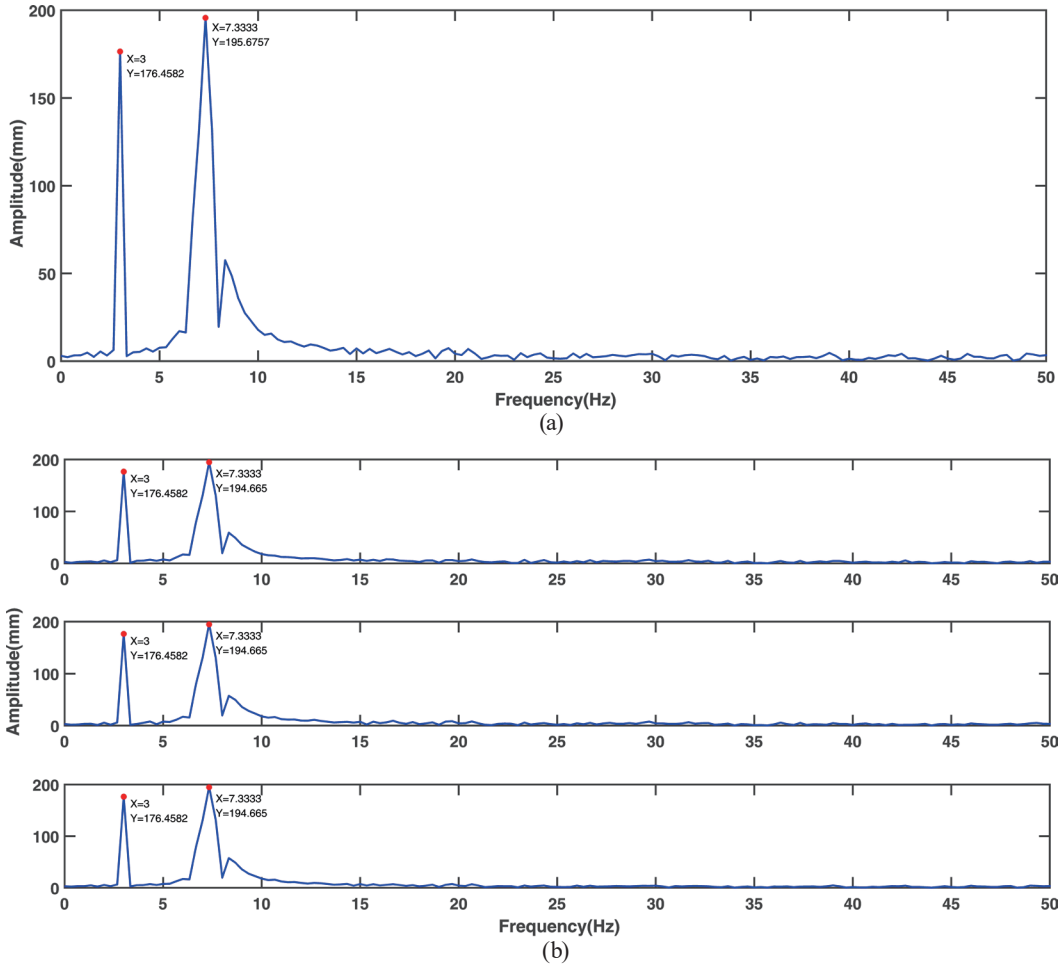

Fig. 7. (Color online) Spectrogram of (a) the simulated signal and (b) multi-channel signals.

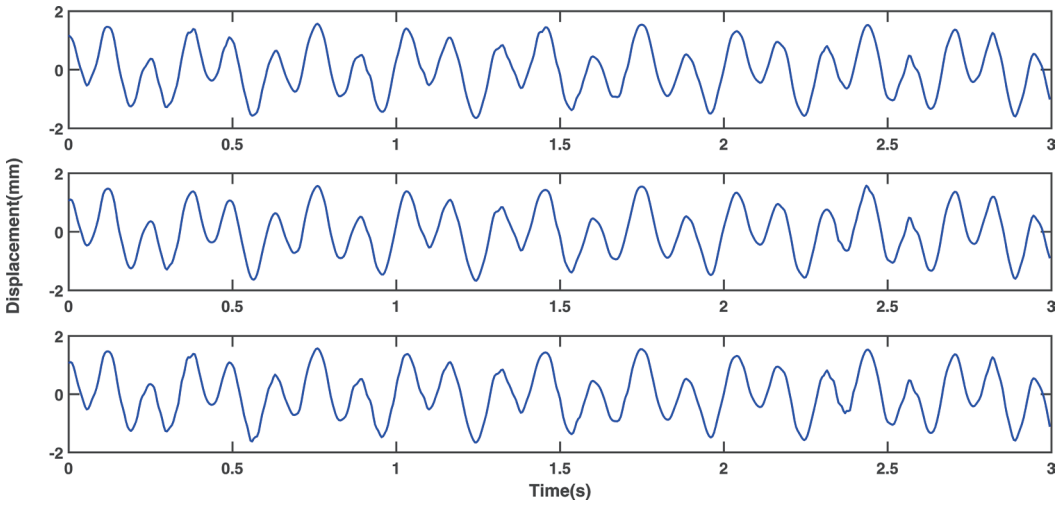

Fig. 8. (Color online) Multi-channel signals after high-frequency noise removal.

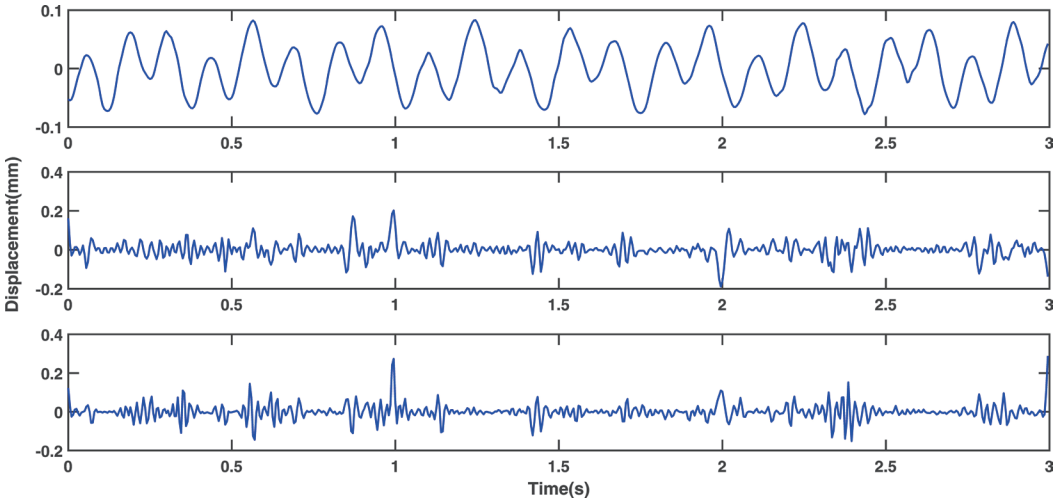

Fig. 9. (Color online) Results of performing SOBI separation on multi-channel signals.

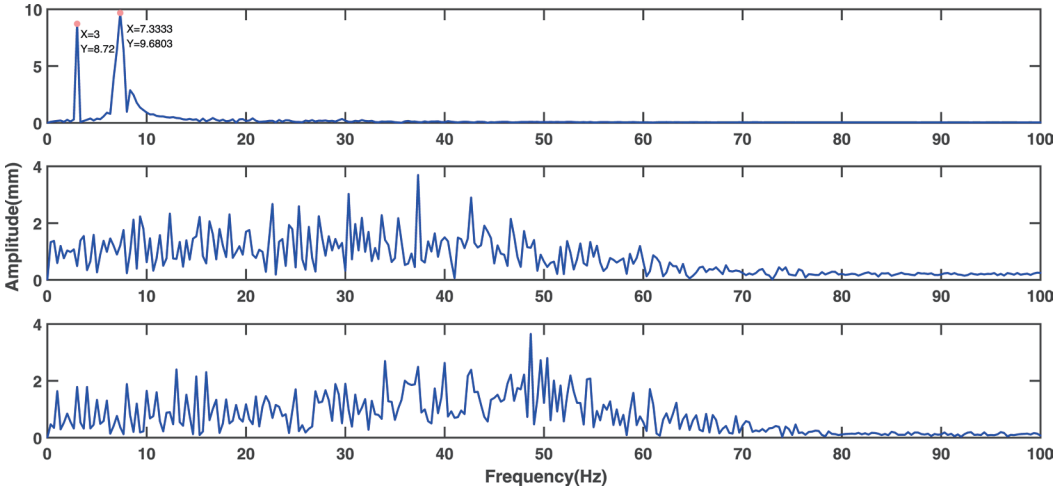

Fig. 10. (Color online) Spectrogram of components obtained by FFT.

Figure 11 shows the denoising effect of the progressive denoising approach. It can be seen from Fig. 11(a) that the signal after denoising was smoother than the original simulation signal $x(t)$. To further illustrate the effect of denoising, Fig. 11(b) shows a comparison between the denoised signal and the useful signal $s(t)$ in the simulation shown in Fig. 3. The two curves were basically consistent in form and highly overlapped. It can thus be seen that the progressive denoising approach can remove noise information and effectively retain useful information.

We used two common indexes, SNR and root-mean-square error (RMSE), to evaluate the denoising effect of the proposed progressive denoising approach:[1,20]

$$SNR = 10\lg\left(\sum_{i=1}^{N}\left(s(i)\right)^2 \Big/ \sum_{i=1}^{N}\left(y(i)-s(i)\right)^2\right), \tag{10}$$

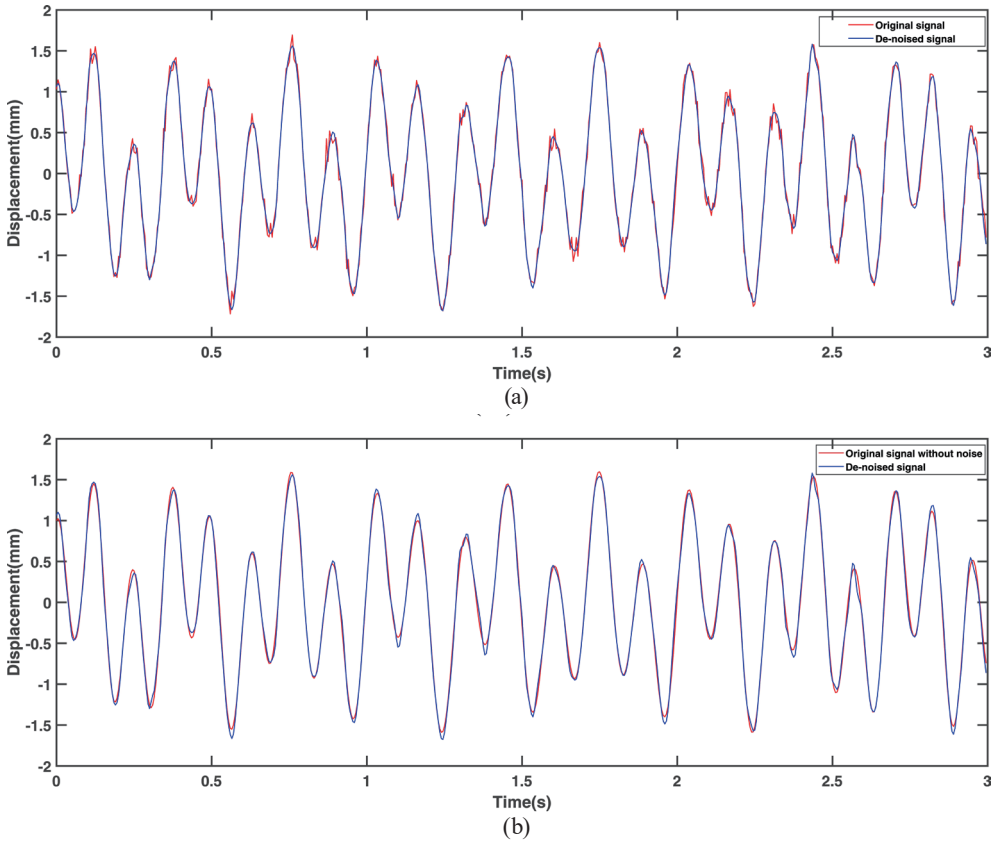

Fig. 11. (Color online) Effect of proposed progressive denoising approach: (a) comparison between $x(t)$ and denoised signal and (b) comparison between $s(t)$ and denoised signal.

$$RMSE = \sqrt{\frac{1}{N}\sum_{i=1}^{N}\left(y(i)-s(i)\right)^2}, \tag{11}$$

where $s(i)$ is the original signal, $y(i)$ is the denoised signal, and N is the number of sampling points.

The SNR and RMSE values of different denoising methods are shown in Table 1. Compared with the original data, the SNR of the progressive denoising approach was increased by 17.02% and the RMSE was reduced by 32.36%, which shows the effectiveness of the proposed progressive denoising approach. In addition, compared with EEMD and ESMD, the proposed approach had improved SNR and RMSE values, showing its superior denoising effect to these methods and further illustrating its feasibility and effectiveness in noise reduction.

3.2 Practical experiment and analysis

Beishatan Bridge is in Haidian District, Beijing. Line 15 of the subway passes under the bridge. There are many buildings such as hotels, schools, and large shopping malls in the

Table 1
Comparison of different denoising methods.

	Raw data	EEMD	ESMD	Proposed method
SNR	20	21.4027	22.8562	23.4032
RMSE	0.0819	0.0698	0.0590	0.0554

(a) (b)

Fig. 12. (Color online) (a) Beishatan Bridge and (b) GB-SAR instrument layout.

surrounding area. The bridge is an important section of the G6 highway connecting the North Fourth Ring Road and the North Fifth Ring Road. Owing to its critical location, Beishatan Bridge is an important transportation hub, making its health monitoring particularly important. Beishatan Bridge consists of two continuous beam bridges with a length of 86.58 m and a width of 12.93 m on the left and right, as shown in Fig. 12(a). In this study, the main span of the right sub-bridge is selected as the research object. To collect real-time dynamic deflection changes of the lower surface of the bridge, the GB-SAR instrument is deployed under the right bridge as shown in Fig. 12(b). The altitude of the instrument is 30°, and the instrument is aligned with a position near the midpoint of the main span of the right bridge. The distance resolution is 0.75 m, the sampling frequency is 200 Hz, and the acquisition time is 60 s.

Figure 13 shows the dynamic time series dynamic deflection signals on the main span midpoint of the right sub-bridge. There was obvious noise interference information in the time series dynamic deflection signals. During the monitoring period, there were six large dynamic deflection changes, which were caused by passing vehicles. The maximum deflection of the right sub-bridge was 1.29 mm. To provide more reliable data support for subsequent bridge health analysis, it was essential to process the noises and improve the accuracy of the Beishatan Bridge monitoring data.

The proposed progressive denoising approach was used to process the original GB-SAR monitoring data of Beishatan Bridge. Figure 14 shows the denoising effect of the proposed approach, where the red curve represents the original monitoring data and the blue curve represents the data after denoising. The proposed denoising approach removed the noise information and retained the useful information characteristics. In particular, it was effective for removing abnormal information at the peaks and troughs.

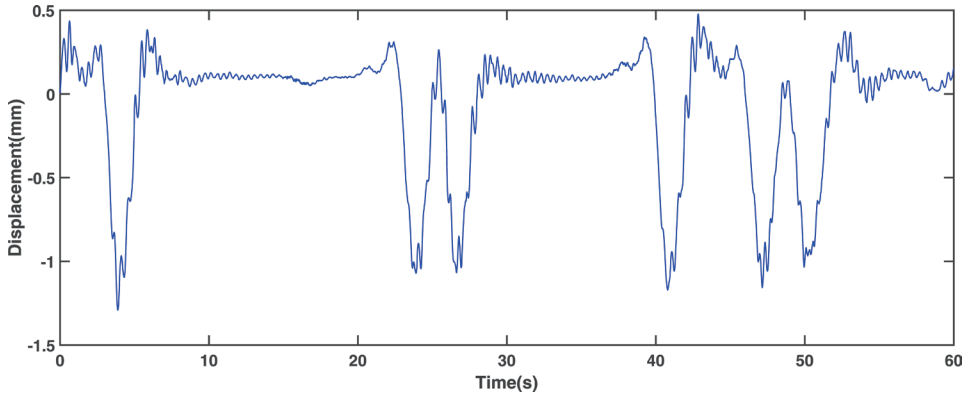

Fig. 13. (Color online) Time series dynamic deflection data on main span midpoint of right sub-bridge.

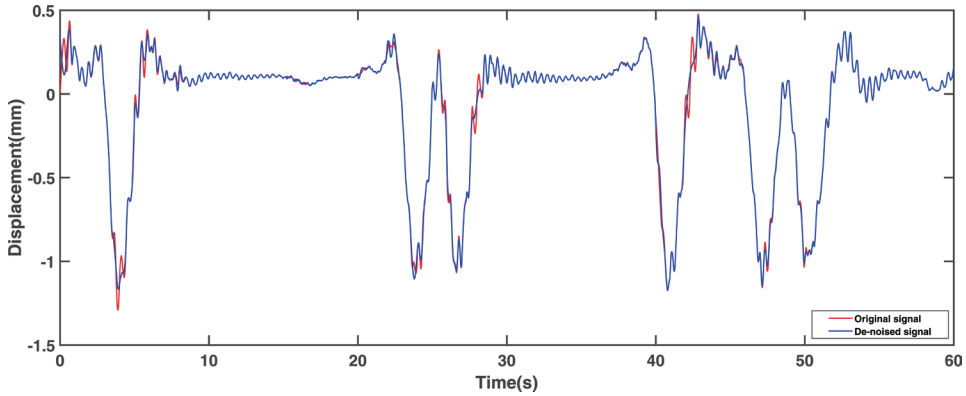

Fig. 14. (Color online) Results of denoising of signal obtained from main span of right Beishatan Bridge.

For real data, the SNR and RMSE are no longer suitable indicators for evaluating the denoising effect. Therefore, we use two different indicators, the noise mode (NM) and the ratio of the variance root (RVR), to comprehensively evaluate the denoising effect of the proposed method from the aspects of energy and graphics. They are expressed as follows:[20]

$$NM = \sqrt{\sum_{i=1}^{N} (y(i) - x(i))^2}, \tag{12}$$

$$RVR = \frac{\sum_{i=1}^{N-1} \left[y(i+1) - y(i) \right]^2}{\sum_{i=1}^{N-1} \left[x(i+1) - x(i) \right]^2}, \tag{13}$$

where $y(i)$ represents the denoised signal, $x(i)$ represents the original signal, and N is the number of sampling points.

The larger the NM value and the closer the RVR value is to zero, the better the denoising effect. By combining these two indicators, the results of denoising can be objectively evaluated and a comprehensive system for evaluating the denoising effect can be realized.

Table 2
Accuracy evaluation of different denoising methods for Beishatan Bridge.

	EEMD	ESMD	Proposed method
NM	0.4305	1.9931	2.1870
RVR	1.1635	0.7708	0.7312

The evaluation index values of denoising accuracy for different denoising methods for the real bridge dynamic time series dynamic deflection signals are shown in Table 2. Compared with EEMD and ESMD, the proposed progressive denoising approach has superior NM and RVR values. In summary, the proposed approach can denoise actual bridge monitoring signals with superior performance to the EEMD and ESMD denoising approaches.

4. Conclusions

For bridge deformation monitoring using GB-SAR, the collected dynamic deflection data is easily subjected to interference by noises due to ground motion and complex traffic factors. Aiming to improve the credibility of dynamic deflection and to ensure the accuracy of bridge safety performance evaluation, we propose a CS-ESMD-based progressive denoising approach. The method can accurately identify useful and noise information of a dynamic deflection signal with different scale frequencies. Through simulation and practical experiments, we obtain the following conclusions:

(1) In the simulation experiment, the SNR of the denoised signal is 23.4032 dB and the RMSE is 0.0554 mm. Compared with EEMD or ESMD alone, the proposed approach achieves higher denoising accuracy. The proposed approach is also shown to be suitable for the denoising processing of nonlinear and nonstationary signals.
(2) In a practical experiment, we show that the proposed method has superior performance to EEMD and ESMD in terms of NM and RVR values, with the NM value increased from 0.4305 and 1.9931 for EEMD and ESMD, respectively, to 2.1870 and the RVR value reduced by 37.2 and 5.1%. The results show the advantageousness of the proposed progressive denoising method.

In summary, the proposed CS-ESMD-based progressive denoising approach can effectively reduce the impact of complex environmental noises on GB-SAR monitoring signals. Improving the accuracy and reliability of bridge dynamic deflection signals is of great significance. The research results have high theoretical importance and application value for the safe operation of bridges.

Acknowledgments

This study was supported by the Ministry of Science and Technology of the People's Republic of China (grant number 2018YFE0206100), the National Natural Science Foundation of China (grant numbers 41871367 and 42171416), the Fundamental Research Funds for Beijing Universities (grant number X20150), the Young Teachers Research Capability Enhancement

Program of Beijing University of Civil Engineering and Architecture (grant number X22019), and the BUCEA Postgraduate Innovation Project (grant number PG2022108).

References

1 X. L. Liu, M. Z Jiang, Z. Q. Liu, and H. Wang: Shock. Vib. **2020** (2020) 1. https://doi.org/10.1155/2020/8430986
2 T. A. Stabile, A. Perrone, M. R. Gallipoli, R. Ditommaso, and F. C. Ponzo: IEEE Geosci. Remote. Sens. Lett. **10** (2013) 870. https://doi.org/10.1109/LGRS.2012.2226428
3 C. Gentile and G. Bernardini: Struct. Infrastruct. Eng. **6** (2010) 521. https://doi.org/10.1080/15732470903068557
4 L. Zhou, J. M. Guo, J. Y. Hu, J. Ma, F. H. Wei, and X. Y. Xue: Int. J. Remote Sens. **39** (2018) 1911. https://doi.org/10.1080/01431161.2017.1416698
5 Z. S. Huang, J. P. Sun, W. X. Tan, P. P. Huang, and K. Y. Han: Sensors **17** (2017) 2950. https://doi.org/10.3390/s17122950
6 D. Tarchi, H. Rudolf, M. Pieraccini, and C. Atzeni: Int. J. Remote Sens. **21** (2000) 3545. https://doi.org/10.1080/014311600750037561
7 S. K. Yadav, R. Sinha, and P. K. Bora: IET Signal Process. **9** (2015) 88. https://doi.org/10.1049/iet-spr.2014.0005
8 O. Ogundipe, J. K. Lee, and G. W. Roberts: J. Appl. Geodesy **8** (2014) 273. https://doi.org/10.1515/jag-2014-0011
9 C. Liu, C. Song, and Q. Lu: J. Appl. Geodesy **144** (2017) 125. https://doi.org/10.1016/j.jappgeo.2017.07.007
10 X. L. Liu, S. N. Li, and X. H. Tong: IEEE J. Sel. Top Appl. Earth Obs. Remote Sens. **11** (2018) 4874. https://doi.org/10.1109/JSTARS.2018.2878482.
11 L. Sendur and I. W. Selesnick: IEEE Trans. Signal Process. **50** (2002) 2744. https://doi.org/10.1109/TSP.2002.804091
12 S. Dong, B. Tang, and Y. Zhang: Measurement **45** (2012) 2052. https://doi.org/10.1016/j.measurement.2012.05.003
13 Z. X. Yang and J. H. Zhong: Entropy **18** (2016) 112. https://doi.org/10.3390/e18040112
14 N. E. Huang, Z. Shen, S. R. Long, M. C. Wu, H. H. Shih, Q. Zheng, N. C. Yen, C. C. Tung, and H. H. Liu: Proc. Math. Phys. Eng. Sci. **454** (1998) 903. https://doi.org/10.1098/rspa.1998.0193
15 Z. H. Wu and N. E. Huang: Adv. Adapt. Data Anal. **1** (2009) 1. https://doi.org/10.1142/S1793536909000047
16 J. W. Li, Y. F. Tong, L. Guan, S. F. Wu, and D. B. Li: RSC Adv. **8** (2018) 8558. https://doi.org/10.1039/C7RA13202F
17 S. Gaci: Energy Procedia **97** (2016) 84. https://doi.org/10.1016/j.egypro.2016.10.026
18 G. Han, B. Lin, and Z. Xu: J. Instrum. **12** (2017) P03010. https://doi.org/10.1088/1748-0221/12/03/P03010
19 Y. F. Lei, W. L. Jiang, H. J. Niu, X. D. Shi, and X. K. Yang: Shock. Vib. **2021** (2021) 1. https://doi.org/10.1155/2021/6649603
20 X. L. Liu, H. Wang, and Y. M. Huang: IEEE J. Sel. Top Appl. Earth Obs. Remote Sens. **14** (2021) 2845. https://doi.org/10.1109/JSTARS.2021.3061543
21 W. C. Xu, Y. H. Hou, Y. S. Hung, and Y. X. Zou: Signal Process. **93** (2013) 261. https://doi.org/10.1016/j.sigpro.2012.08.005
22 W. C. Xu, C. R. Chen, J. S. Dai, Y. Z. Zhou, and Y. Zhang: Signal Process. **161** (2019) 165. https://doi.org/10.1016/j.sigpro.2019.03.017
23 A. Belouchrani, K. Abed-Meraim, J. F. Cardoso, and E. Moulines: IEEE Trans. Signal Process. **45** (1997) 434. https://doi.org/10.1109/78.554307
24 F. Miao, R. Z. Zhao, L. L. Jia, and X. L. Wang: Appl. Sci. **10** (2020) 3735. https://doi.org/10.3390/app10113735
25 M. Schneider: Acta Mech. **232** (2021) 2051. https://doi.org/10.1007/s00707-021-02962-1